ECS Transactions, 41 (1) 679-687 (2011)
10.1149/1.3635602 ©The Electrochemical Society

Microstructure Analysis Tools for Quantification of Key Structural Properties of Fuel Cell Materials

A. Cecen[a], E. A. Wargo[a], A. C. Hanna[a], D. M. Turner[b],
S. R. Kalidindi[a,b], E. C. Kumbur[a,*]

[a] Department of Mechanical Engineering and Mechanics, Drexel University, Philadelphia, Pennsylvania 19104, USA
[b] Department of Materials Science and Engineering, Drexel University, Philadelphia, Pennsylvania 19104, USA
[*] Corresponding author (kumbur@drexel.edu)

The objective of this work is to develop advanced microstructure analysis tools for direct quantification of the key structural properties of complex fuel cell materials. Computationally efficient algorithms have been developed to extract the key structural parameters from measured microstructure datasets of these materials. In addition to determination of the traditional structural measures (e.g., porosity, surface area, phase connectivity), two novel microstructure analysis techniques are introduced for the quantification of pore size and tortuosity distributions. For initial demonstration purposes, the methods developed are applied to a digitally reconstructed sample of the micro-porous layer (MPL) of a polymer electrolyte fuel cell (PEFC). The results produced from these analyses are compared to previously reported experimental and model-derived values where applicable.

Introduction

The performance and durability of fuel cells are strongly linked to the materials used in these systems (1). However, experimental quantification of the key properties of these materials can be expensive and quite difficult to conduct. To date, most standard experimental methods (e.g., porosimetric techniques) are limited to provide bulk property data which only indicate the general characteristics of the material. However, many fuel cell materials exhibit strong heterogeneity with anisotropy in properties, whose rigorous quantification requires measurements in multiple directions and locations. Therefore, it is imperative to develop microstructure analysis tools to accurately capture the myriad features and spatial variations of the key transport properties in these materials.

To date, fundamental image analysis techniques have been widely used to estimate common structural parameters including phase-specific volume fraction (e.g., porosity), connectivity, and internal surface area of complex materials. However, the direct methods or computational protocols to estimate the tortuosity and pore size distribution are only vaguely mentioned in current literature. Notably, Wu *et al.* (2) describes a method based on a modified A* search algorithm to find relative path lengths as a measure for tortuosity in digitally reconstructed sodium chloride compacts. While this method brings a new perspective to evaluate the tortuosity, it is limited to perform analysis in 2-D

datasets, and therefore is not capable of capturing the bidirectional transport in a 3-D microstructure dataset. Similarly, Zils *et al.* (3) utilized a geometric method to calculate tortuosity for PEFC catalyst layer samples, but the results are limited to estimate only a single "average" value for tortuosity. Regarding pore size distribution, a recent effort by Zielger *et al.* (4) reported the use of an idealized geometry approach to determine the pore size distribution of the PEFC catalyst layer. While the presented approach enables accurate analysis of homogeneous porous structures in 3-D, the use of spherical assumptions to quantify the void space most likely misrepresents the jagged morphology of complex fuel cell materials such as diffusion media. To the best of the authors' knowledge, a direct method to quantify the true geometrical shapes of the pore space in fuel cell materials has not been developed or successfully implemented.

The focus of this study is to introduce direct methods for extracting key structure metrics (properties) of fuel cell materials. Two novel microstructure analysis protocols are introduced for the quantification of the tortuosity and pore size distributions. Firstly, a novel shortest path search method is developed to identify all of the tortuous paths and compute the spatial distribution of tortuosity for a given microstructure dataset. Secondly, new methods are introduced to quantify the statistics of the connected-pore space using orientation-resolved chord length distributions. In an effort to demonstrate their potential utility, these methods are applied to the micro-porous layer (MPL) of a PEFC.

Methods and Computational Procedures

Dataset Acquisition and Image Processing

The MPL of a SIGRACET® SGL 10BC gas diffusion layer was selected for initial demonstration of the presented methods. Due to the relatively small pore sizes, focused ion beam scanning electron microscopy (FIB-SEM) was chosen to capture the internal structure of the tested MPL sample in 3-D. An FEI Strata™ DB 235 FIB-SEM was utilized to quantify an MPL volume of ~5x8x2 μm by serial sectioning with an image resolution of ~10 nm and slice thickness of 20 nm (Fig. 1a).

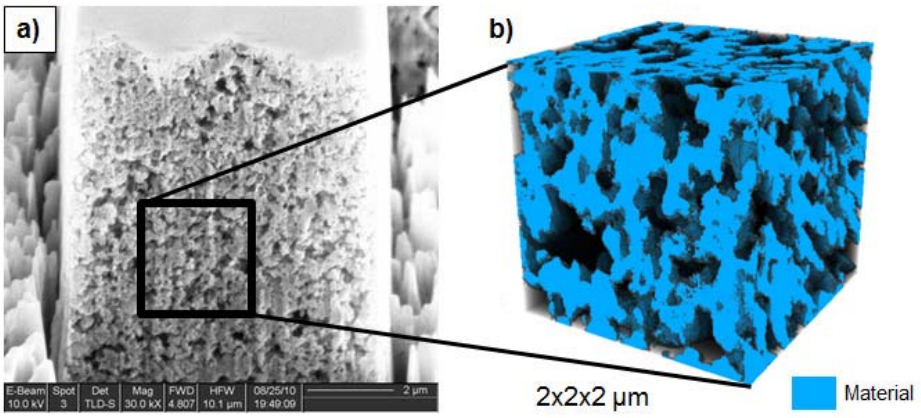

Figure 1. a) A slice of the MPL as captured by the SEM. b) 3-D digital reconstruction of the designated section of the MPL.

Following the image acquisition, the data is corrected for possible inaccuracies resulting from the FIB-SEM setup. First, the data is realigned using a Fourier transform registration code. Then, it is shifted/stretched to compensate for the viewing angle of the SEM. Finally, the shadow gradient in each image is removed by finding a bi-parabolic fit for the gradient and dividing the image data by the fitted bi-parabolic surface. The bi-parabolic fit for each image was computed using the surface fitting method proposed by Pastushenko (5). Next, the data is segmented using the ISODATA thresholding technique (6-8). The resulting segmented images were then stacked to create a 3-D binary image (i.e., digital structure dataset) of the internal structure of the MPL sample. This 3-D structure dataset was then further analyzed to remove any material islands (i.e., residuals) that appear to be floating in void space. The resulting binary 3-D structure dataset (example shown in Fig. 1b) was used to determine key structure metrics of the MPL (e.g., porosity, connectivity, surface area, tortuosity distribution etc.).

Quantification of Porosity, Surface Area and Connectivity

Fundamental image analysis techniques were applied to estimate phase-specific volume fraction (e.g., porosity), total internal surface area, and connectivity. As the first step, porosity was estimated as the ratio of the number of pore voxels to the total number of voxels in the 3-D MPL microstructure dataset. Next, total surface area was estimated using matrix shifting to detect boundaries in directions along the main axes. The number of boundary voxels identified in a given direction was multiplied by the surface area of a voxel face in that direction. The resulting surface area values for each direction were summed and then divided by the size of the analyzed volume to estimate the surface area per unit volume. Subsequently, connectivity was estimated by identifying the connected components within the pore space. Any pore voxels that are connected to both the starting surface and the destination surface (e.g. the opposing surfaces along the through-plane direction) were identified as the "connected-pore" phase. The ratio of the number of connected-pore voxels to the total number of pore voxels was defined as the pore connectivity.

Determination of Tortuous Paths and Tortuosity Distribution

A special algorithm was developed to identify all of the tortuous paths existing within a selected 3-D digital microstructure dataset. This method uses Dijkstra's algorithm (9) to search for the shortest path from an entry point on the start surface to any point on the end surface. To implement this algorithm, the given 3-D structure dataset is transformed into a 2-D adjacency matrix, where the structure is depicted as a mathematical graph. Each node in the graph represents a voxel (pore or solid in the case of the MPL), and each link represents a physical connectivity between the two voxels. The link between any two pore voxels has a numerical value representing the Euclidean distance between the two. The search algorithm then finds the shortest possible path from a designated starting node to any end node on the opposing surface. Performing the shortest path calculation for every single pore voxel on the start surface automatically identifies all of the tortuous paths of interest. The length of each tortuous path is then divided by the distance separating the start and end faces to estimate the corresponding tortuosity values. The tortuosity distribution obtained using this method can be used to determine various tortuosity related statistics (e.g., mean, median, mode, standard deviation). To the best of the authors' knowledge, these statistics cannot be determined by the methods previously

reported in literature. It is anticipated that the large quantity of statistics obtained using this approach will lead to a deeper insight into the precise role of this key structure metric in influencing the bulk transport properties.

Chord Length Distribution – An Alternative Conceptualization of Pore Size Distribution

Here, we introduce the concept of chord length distribution as an alternative parameter to the commonly used pore size distribution concept to better represent the shape and size distribution of the pore space in complex microstructures. A chord is defined as a line of specific orientation which connects two phase boundaries within a material structure while lying completely within a single material phase (i.e., chords are not allowed to cross phase boundaries) (see Fig. 2). Therefore, the start and end points of a chord are located at the phase boundaries and form a pair of points that define the chord for a given orientation. The length 'c' of a chord is estimated by the Euclidean distance between the boundary pixel pair. This operation is repeated for desired directions and throughout every boundary pixel pair to produce a chord length dataset, which represents the chord length distribution. The chord length analysis is applied to a particular phase of interest to determine the chord length distribution for that phase. In this study, the pore phase was analyzed to obtain the pore size and shape distribution for the tested MPL sample.

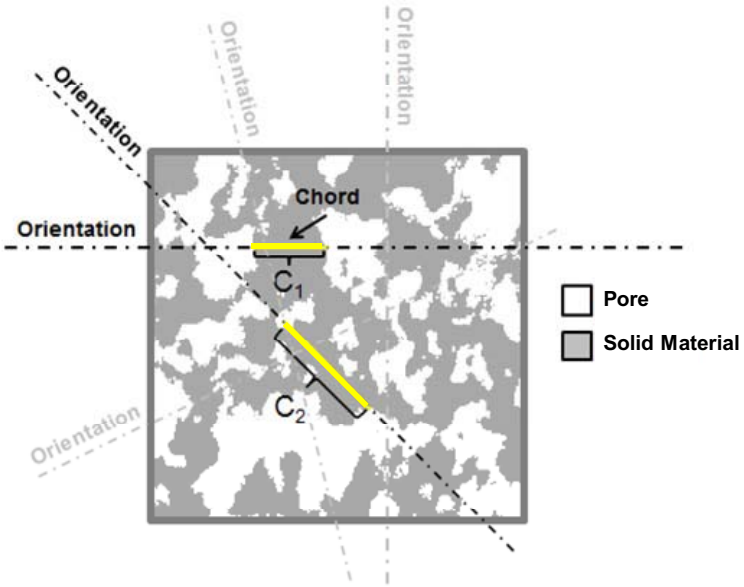

Figure 2. Sample chords of lengths 'c_1' and 'c_2' at sample orientations, as well as examples of other possible orientations, are shown on a cross-section of the MPL microstructure. The chords shown in the hypothetical structure are for the solid material phase; however, it can be performed on the pore space as well.

The chord length distribution described above presents a much more rigorous and meaningful representation of the pore size and shape distribution compared to the currently used concept of pore-size distribution. Once again, a number of statistics (e.g., mean, median, mode, standard deviation) can be extracted from each chord-length distribution. It is also important to note that the chord length distribution can be extracted in different directions for a given 3-D structure dataset, which allows one to quantify the anisotropy of the pore size and shape distribution. For the MPL microstructure studied

here, chord length distributions were extracted only for the pore phase in the three primary orthogonal directions.

Results and Discussion

Estimation of Key Structural Properties

The metric analyses were performed on sets of small volumes (each 100x100x100 pixels, ~ 1x1x1μm) within the full dataset of 800x500x200 pixels, in order to reduce computational cost. In addition to sets of 100, 200 and 300 random volumes, a set composed of 80 non-overlapping volumes was also analyzed. Table I shows the key structure metrics (porosity, total surface area, and pore connectivity) for the four different groups of datasets obtained from the MPL sample. The results show very small variation (less than 5%) between the predicted values of the properties for each group, indicating that the material structure is sufficiently sampled. Here, we have emphasized the set of 80 non-overlapping volumes for further analysis of the results.

Table I. The key structural properties of the MPL estimated using sets composed of different numbers of volumes, each 100x100x100 pixels^3 (~ 1 μm^3).

Metrics	Number of Volumes				Units
	80	100	200	300	
Porosity	0.41±0.04	0.41±0.04	0.41±0.04	0.42±0.04	Fraction
Total Surface Area	23.94±2.70	24.13±2.80	24.08±2.46	24.21±2.64	$\mu m^2/\mu m^3$
Pore Connectivity	0.99±0.003	0.99±0.003	0.99±0.003	0.99±0.003	Fraction

For all 80 selected volumes, the connected component search algorithm predicts the connectivity of the pores as 99% ± 0.3%, indicating that almost the entire pore volume is a single highly connected pore network with very few isolated pores. Therefore, it is very likely that a similar level of pore connectivity can be seen in the entire MPL sample. The results indicate an overall porosity of 0.42±0.04 for the tested MPL sample. These results are in good agreement with reported values in literature, which indicate porosity values between 0.4 and 0.6 for the MPL (10-13).

Tortuosity Distribution

Using the previously described shortest path algorithm, the tortuosity distributions for each of the 80 non-overlapping volumes were computed. These distributions were summed and normalized to yield a cumulative tortuosity distribution corresponding to the entire dataset (i.e., the full 3-D image of size 800x500x200 pixels). An example of the simulation for a member of the 80 non-overlapping volumes set and the cumulative tortuosity distribution is shown in Fig. 3. It can be inferred from the cumulative distribution that the majority of the tortuosity values are between 1.1 to 1.6 for the tested MPL, with an effective (average) value of 1.33 and mode of 1.26. These results, along with the distribution in Fig. 3, show that the tested MPL microstructure contains a broad range of tortuous paths with different lengths, which suggests that the use of a "single" effective tortuosity value alone may mislead the representation of tortuous structure of the fuel cell material, and therefore lead to an inaccurate estimation of the transport

characteristics of the material. An appropriate approach, however, would be to represent the tortuous structure as a distribution (Fig. 3), where one can closely observe the trend and peaks in tortuous paths to identify the local regions that are highly resistive to the species transport. In terms of comparison, a recent study by Ostadi *et al.* (10) reported the through-plane tortuosity value for an MPL as 1.36, which shows a good agreement with the average value (~ 1.33) predicted in this study.

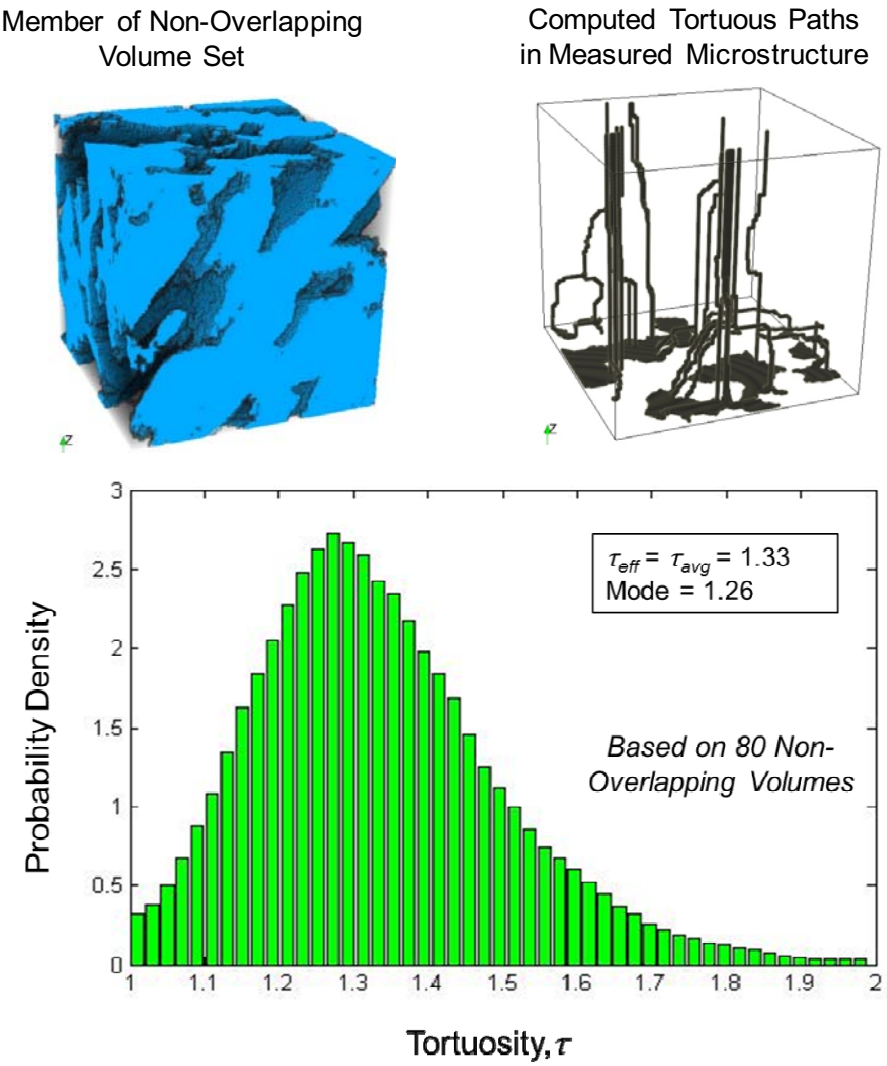

Figure 3. Tortuosity simulation for a volume selected from the full dataset and the cumulative tortuosity distribution based on the data computed for 80 non-overlapping volumes.

Chord Length Distribution

The chord length distribution algorithm was applied to the *full dataset* (800x500x200) by using the three primary orthogonal directions (x, y and z) as the possible chord orientations to capture the size of the pore space within the MPL microstructure. The resulting chord length distribution is shown in Fig. 4. As mentioned earlier, the concept of a chord length distribution is not based on the assumption of idealized circular/spherical geometries as it is in conventional pore size analysis, therefore a more accurate detection of pore geometry and size can be achieved with high resolution.

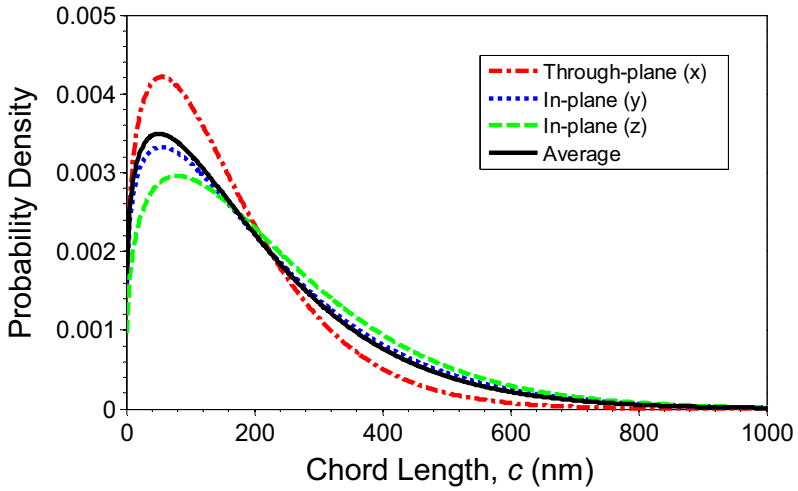

Figure 4. Chord length distributions for the pore phase of the full MPL microstructure dataset in the three primary orthogonal directions.

In addition to the identification of pore size and distribution within the microstructure, the computed chord length data can be used to calculate dominant length scales to determine the mode of transport within the microstructure. For instance, with the chord length distribution data, one can calculate the Knudsen number and its distributions for hydrogen, oxygen, and water vapor in the MPL (Fig. 5). The Knudsen number, Kn, is defined as the dimensionless ratio of the mean free path of fluid particles, λ, to the representative length scale, L (14):

$$\mathrm{Kn} = \lambda / L \qquad [1]$$

In this case, L is taken to be the chord length, and λ is calculated for each species based on kinetic theory and by assuming an average relative particle velocity (15-18). The Knudsen number distributions shown in Fig. 5 indicate that the majority of diffusion in the MPL for all three gas species falls in the transition region between continuum/slip flow and free-molecule flow ($0.01 < \mathrm{Kn} < 10$), where both Fickian and Knudsen diffusion are prominent (19-20).

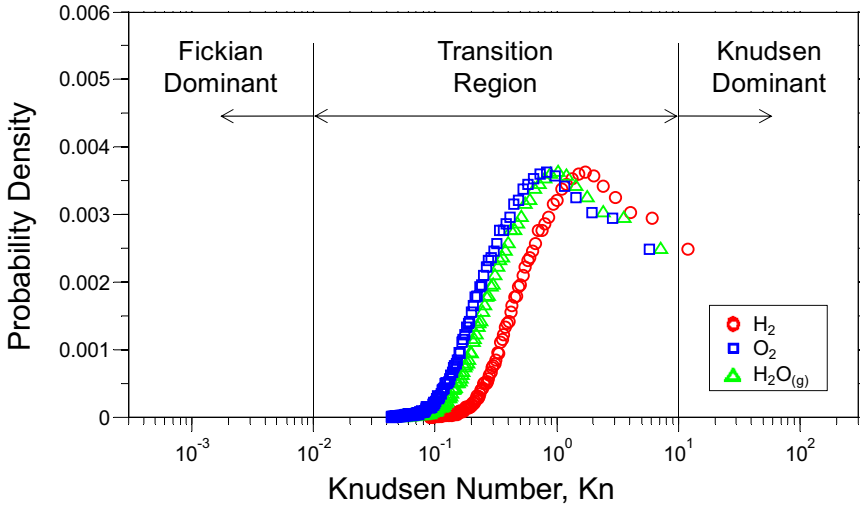

Figure 5. Knudsen number distributions for hydrogen, oxygen, and water vapor in the MPL at 80 °C and 1 atm, based on the average chord length distribution.

Summary and Conclusions

In this study, novel microstructure analysis tools for the estimation of key structure-related metrics of porous fuel cell materials were described. For initial demonstration, these methods were applied to a 3-D microstructure dataset of an MPL substrate of a PEFC. Two new metrics, namely chord length distribution and tortuosity distribution, were introduced. Rather than a single tortuosity value, representation of the tortuous paths as a "distribution" is shown to be more effective to better understand the spatial variation of microstructure and the tortuous nature of fuel cell materials. Secondly, the chord length distribution metric is introduced as an alternative concept for describing the pore size distribution for this class of materials. This new metric represents the orientation and size related statistics of a desired phase (e.g., pore, solid) in a 3-D microstructure dataset, and allows for more accurate analysis of irregular pore geometries in complex microstructures, where defining a pore and its size is highly ambiguous such as in most fuel cell materials. The chord length analysis also enables direct quantification of the specific path lengths, which can be used for determination of the dominant diffusion mode within the microstructure of the material.

Acknowledgments

This work was partially supported by the U.S. Department of Education's GAANN program (Award#P200A100145) and the National Science Foundation (Grant #1066623). The authors would also like to thank Dr. Craig L. Johnson (Centralized Research Facilities, Drexel University) for his guidance in FIB-SEM operation.

References

1. R. Borup, J. Meyers, B. Pivovar, Y. S. Kim, R. Mukundan, N. Garland, D. Myers, M. Wilson, F. Garzon, D. Wood, P. Zelenay, K. More, K. Stroh, T. Zawodzinski, J. Boncella, J. E. McGrath, M. Inaba, K. Miyatake, M. Hori, K. Ota, Z. Ogumi, S. Miyata, A. Nishikata, Z. Siroma, Y. Uchimoto, K. Yasuda, K. Kimijima, N. Iwashita, *Chemical Reviews*, **107**, 3904 (2007).
2. Y. S. Wu, L. J. van Vliet, H. W. Frijlink, K. van der Voort Maarschalk, *European Journal of Pharmaceutical Sciences,* **28**, 433 (2006).
3. S. Zils, M. Timpel, T. Arlt, A. Wolz, I. Manke, C. Roth, *Fuel Cells*, **10**, 966 (2010).
4. C. Ziegler, S. Thiele, R. Zengerle, *Journal of Power Sources*, **196**, 2094 (2011).
5. V. Pastushenko, Surfit (http://www.mathworks.com/matlabcentral/fileexchange/6244), MATLAB Central File Exchange, (18 Nov 2004).
6. G. H. Ball, D. J. Hall, Stanford Research Institute, Menlo Park, CA, Technical Report AD 699616 (1965).
7. T. W. Ridler, S. Calvard, *IEEE Transactions on Systems, Man, and Cybernetics*, **SMC-8**, 630 (1978).
8. D. Ramachandram, Automatic Thresholding (http://www.mathworks.com/matlabcentral/fileexchange/3195), MATLAB Central File Exchange, (31 Mar 2003).
9. E. W. Dijkstra, *Numerische Mathematik,* **1**, 269 (1959).

10. H. Ostadi, P. Rama, Y. Liu, R. Chen, X.X. Zhang, K. Jiang, *Journal of Membrane Science*, **351**, 69 (2010).
11. J. Becker, C. Wieser, S. Fell, K. Steiner, *International Journal of Heat and Mass Transfer*, **54**, 1360 (2011).
12. K. T. Cho, M. M. Mench, *Journal of Power Sources*, **195**, 6748 (2010).
13. H. Tang, S. Wang, M. Pan, R. Yuan*, Journal of Power Sources*, **166**, 41 (2007).
14. K. Jiao, X. Li, *Progress in Energy and Combustion Science*, **37**, 221 (2011).
15. Mean free path, molecular collisions, 16 June 2011, (http://hyperphysics.phy-astr.gsu.edu/hbase/kinetic/menfre.html).
16. N. M. Laurendeau, *Statistical Thermodynamics: Fundamentals and Applications*, Cambridge UP, Cambridge (2005).
17. A. Bondi, *J. Phys. Chem.*, **68**, 441 (1964).
18. B. Cordero, V. Gómez, A. E. Platero-Prats, M. Revés, J. Echeverría, E. Cremades, F. Barragán, S. Alvarez, *Dalton Trans.*, **21**, 2832 (2008).
19. X. Chen, E. Pfender, Plasma *Chemistry and Plasma Processing*, **3**, 97 (1983).
20. L. P. Yarin, A. Mosyak, G. Hetsroni, *Fluid Flow, Heat Transfer and Boiling in Micro-Channels*, Springer, Berlin/London, (2008).